Computers & Geosciences 103 (2017) 152–163

Contents lists available at ScienceDirect

Computers & Geosciences

journal homepage: www.elsevier.com/locate/cageo

Case study

Augmenting comprehension of geological relationships by integrating 3D laser scanned hand samples within a GIS environment

A.S. Harvey[a,*], G. Fotopoulos[a], B. Hall[b], K. Amolins[b]

[a] Queen's University, Department of Geological Sciences and Geological Engineering, 36 Union Street, Kingston, Ontario, Canada, K7L3N6
[b] Esri Canada, 12 Concorde Place Suite 900, Toronto, Ontario, Canada, M3C3R8

ARTICLE INFO

Keywords:
3D laser scanner
Geology
GIS
Web GIS
Virtual database
Rocks
Minerals

ABSTRACT

Geological observations can be made on multiple scales, including micro- (e.g. thin section), meso- (e.g. hand-sized to outcrop) and macro- (e.g. outcrop and larger) scales. Types of meso-scale samples include, but are not limited to, rocks (including drill cores), minerals, and fossils. The spatial relationship among samples paired with physical (e.g. granulometric composition, density, roughness) and chemical (e.g. mineralogical and isotopic composition) properties can aid in interpreting geological settings, such as paleo-environmental and formational conditions as well as geomorphological history. Field samples are collected along traverses in the area of interest based on characteristic representativeness of a region, predetermined rate of sampling, and/or uniqueness. The location of a sample can provide relative context in seeking out additional key samples. Beyond labelling and recording of geospatial coordinates for samples, further analysis of physical and chemical properties may be conducted in the field and laboratory. The main motivation for this paper is to present a workflow for the digital preservation of samples (via 3D laser scanning) paired with the development of cyber infrastructure, which offers geoscientists and engineers the opportunity to access an increasingly diverse worldwide collection of digital Earth materials. This paper describes a Web-based graphical user interface developed using Web AppBuilder for ArcGIS for digitized meso-scale 3D scans of geological samples to be viewed alongside the macro-scale environment. Over 100 samples of virtual rocks, minerals and fossils populate the developed geological database and are linked explicitly with their associated attributes, characteristic properties, and location. Applications of this new Web-based geological visualization paradigm in the geosciences demonstrate the utility of such a tool in an age of increasing global data sharing.

1. Introduction

Geological interpretation and comprehension is optimally achieved with first hand access and exposure to data and Earth materials. However, spatio-temporal observable geological processes and materials that are directly observable by humans are narrow relative to the entire scale across which geological processes and Earth materials occur. Additionally, there are many scenarios where immediate access to meso-scale (< m) and macro-scale (> km) data is unattainable. This is particularly evident in educational environments where field visits are cost-prohibitive and in cases where field sites of interest are located in remote areas. Hence, there is a need for tools in geology that overcome these obstacles, which in part motivated this research. In addition, there has been growing interest in the applicability of unifying data to reduce subjectivity and bias while presenting information in a comprehensible manner for various users (Sivarajah et al., 2014). It should be noted that the digitization of Earth materials is emphasized here over observable geological processes.

In this paper, the intersection of geovisualization and 3D acquisition is explored. Geovisualization itself involves the intersection between information visualization and scientific visualization, where geospatial information is communicated in ways that emphasize knowledge construction through interaction (MacEachren and Kraak, 1997). Some relevant tools and techniques have been introduced thus far through interdisciplinary literature. MacEachren et al. (2004) present an overview of geovisualization, focusing on its functions: task types, user types, and interaction level. As a result of the interdisciplinary nature of the field, literature tends to limit scopes and a universal framework for understanding how geovisualization works across the spectrum has not been formally codified (Çöltekin et al., 2016). Examples of direct geovisualization applications include assessing mineral resources with a 3D visualization system (Qiu et al., 2015) and geotechnical site investigation (Yeniceli and Ozcelik, 2016). Other examples include exploring how volume graphics and big data are used in geological interpretation (Byers and Woo, 2015) and advancing field

* Corresponding author.
E-mail addresses: 8ash5@queensu.ca (A.S. Harvey), gf26@queensu.ca (G. Fotopoulos), bhall@esri.ca (B. Hall), kamolins@esri.ca (K. Amolins).

http://dx.doi.org/10.1016/j.cageo.2017.02.008
Received 25 May 2016; Received in revised form 13 February 2017; Accepted 14 February 2017
Available online 17 February 2017

techniques (Whitmeyer et al., 2010; Jordan and Napier, 2016). Approaches using open source and common software, such as Google Earth and Microsoft Excel, are being developed to promote accessibility and further collective technical advancement in this realm (Blenkinsop, 2012). Literature widely focuses on macro-scale applications using LiDAR. As we approach the meso-scale part of the spatial spectrum, new challenges arise. The British Geological Survey has compiled a database of type specimen fossils (British Geological Survey, 2016) and De Paor (2016) explored research similar to this which involves georeferencing "virtual rocks" using Google Earth. 3D digital geological samples have been used to monitor the effect of changes in rock microstructure on the permeability by measuring flow through the samples, which can be repeated virtually infinitely through the use of a 3D printer (Head and Vanorio, 2016). All of these relevant efforts in geovisualization have contributed to a paradigm shift that has been years in the making.

3D data acquisition can be achieved in a number of ways such as optical/photogrammetry, radar, thermal, structure from motion, and acoustic techniques (Westoby et al., 2012; Zlatanova, 2008). This research focuses on acquisition by laser scanning, where a directed laser takes distance measurements. Non-contact laser scanning is achieved through time-of-flight, phase-shift, or triangulation. In time-of-flight systems, the length of time for the laser to hit a target and reflect back to a sensor is used to calculate the distance the laser travelled given the known speed of light. In phase-based systems, a laser emits multiple phases and uses phase-shift of the return to determine distance from the scanner. In triangulation, a source emits a laser at a given angle and the laser's location is detected by a sensor. The angle, location, and known baseline distance between source and sensor are used to determine the laser's position in 3D space. Triangulation systems are well suited for range images with smaller scanner-target distances, and are thus useful in digitizing meso-scale hand samples as demonstrated herein.

Desktop 3D acquisition technology has recently become more accessible to a wider demographic, and has seen an increasing number of practical applications (see for example Khoshelham and Elberink, 2012) including, glaciology and bathymetry studies (Mankoff and Russo, 2013) and granulometric analysis in sedimentology (Chávez et al., 2014). Laser scanners capable of capturing data at high resolutions have been used to estimate geological surface roughness (Mills and Fotopoulos, 2013) and point clouds captured by other means have been used to detect anisotropic features on rock surfaces (Baker et al., 2008). 3D scanning technology has also seen applications in morphometric analysis of archeological artifacts (Lin et al., 2010) and rock art (Domingo et al., 2013). Some paleontologists have embraced scanning technology as a non-invasive method of preserving samples (Bates et al., 2010; Contessi and Fanti, 2012; Fanti et al., 2013). It has been asserted that the development of a 3D digital database system would greatly benefit paleontology and archeology by allowing faster and more cost-effective digital transfer of samples (Bates et al., 2010; Betts et al., 2011), which would also have great implications for analysis and museum conservation practices (Kuzminsky and Gardiner, 2012).

With the rapid development of these databases containing vast amounts of information, it is important to develop tools concurrently that are capable of reading, manipulating, and presenting these data in a comprehensible platform, which in fact is the focus of this paper. Students of geology can find abstract concepts of Earth systems models difficult to understand (King, 2008) and entry into science, technology, engineering and mathematics (STEM) fields tends to favour those who are more proficient in spatial abilities (Uttal and Cohen, 2012). Though domain specificity of transferrable skills has been observed regarding visuospatial abilities (Sims and Mayer, 2002), relevant training can be used to augment these abilities to higher levels (Sanchez, 2012).

This paper addresses contextualization of 3D meso-scale samples through blending macro-scale geological and geophysical images. Well-established practices in image blending are rooted in digital compositing, involving the combination of several images' components into a single image (Porter and Duff, 1984). Various types of blending, such as linear interpolation and opacity modification, are common approaches. Disciplines utilizing and developing data and image blending techniques range from medicine (e.g. Cai and Sakas, 1999) to geological exploration (Kovesi et al., 2014) and visualization approaches, such as this work.

The main objectives of this paper are (i) the development of a digital 3D library storage protocol featuring direct import, export, and editing compatibility with ArcGIS, (ii) the development of a "bringing the field to you" experience in which 3D digitally scanned Earth samples are placed within geological and geographical context via a georeferencing protocol within 2D and 3D ArcGIS environments, and (iii) the ability to incorporate data from various internal and external sources, allowing for a customized search experience. The developed tools are based on the following five principles of 3D visualization, namely (i) to provide multiple representations and descriptions, (ii) make linked referential connections visible, (iii) present the dynamic and interactive nature of geology, (iv) promote the transformations between 2D and 3D, and (v) reduce cognitive load by making information explicit and integrated (adapted from Wu and Shah (2004)).

2. Methodology

The proposed approach and realization of these data visualization techniques is achieved through the use of three platforms, namely ArcGIS Online, Web AppBuilder for ArcGIS (Developer Edition) v1.3, and ArcGIS API for Javascript v3.15. Using these platforms and tools allow for effective data management, customization of widgets and themes, and a unified interface that is ideal for multi-scale visualization. Three main sections describe and demonstrate the developed tools, namely (1) meso-scale sample acquisition and digitization, (2) custom widget development, and (3) two case studies illustrating widget utility.

2.1. Meso-scale sample acquisition and digitization

Earth and rock samples collected during field expeditions serve to advance the geological understanding of regions of interest and facilitate interpretation. The metadata required for each sample depend on the objectives of the expedition and overall project. In a recent US Geological Survey (USGS) report on the Geologic Collections Management System (USGS, 2015), the minimum requirements for a collected sample to be retained include a unique identifier (ID) and geographic coordinates. Newer samples require additional information, such as the date of collection. Field geologists have used digital workflows for several decades. A recent effort to facilitate discussion among field-based geologists and computer scientists specializing in databases is the Earth-Centered Communication for Cyberinfrastructure (EC3) project (Mookerjee et al., 2015). Fig. 1 summarizes the different types of metadata that were identified as useful for geoscientists to capture as part of a standard workflow both in the field and laboratory settings. For more detailed lists, refer to Mookerjee et al. (2015).

The development of virtually linked and networked databases for samples can be augmented through the use of digitization of samples. Other techniques for digitization exist as was briefly mentioned in the introduction. The storage and management of such a vast collection of physical rock samples and metadata is an enormous undertaking. 3D scanning of the meso-scale samples may be conducted for preservation and in order to perform further scientific/numerical analyses. The achievable data quality and ease of using laser scanning technology lends itself to this particular application as is demonstrated below. The 3D scanning process is summarized in Fig. 2. Hand samples used in

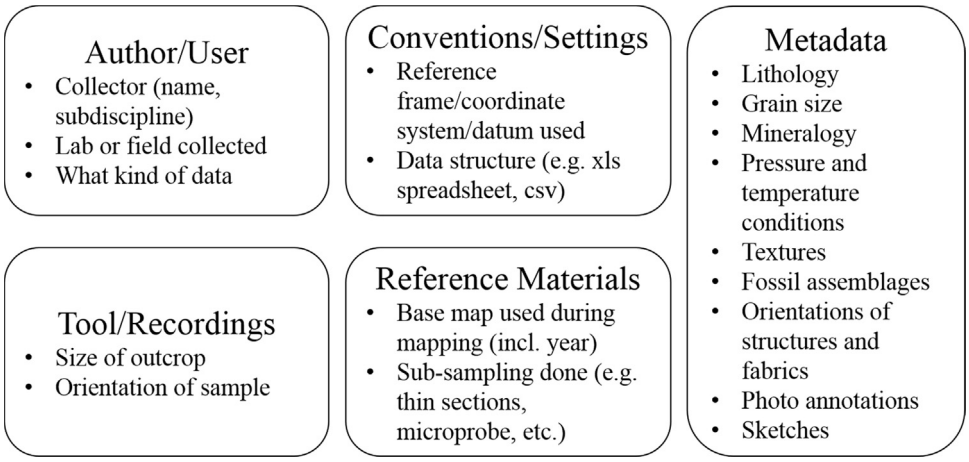

Fig. 1. Summary of metadata and data often collected by field geologists, adapted from Mookerjee et al. (2015).

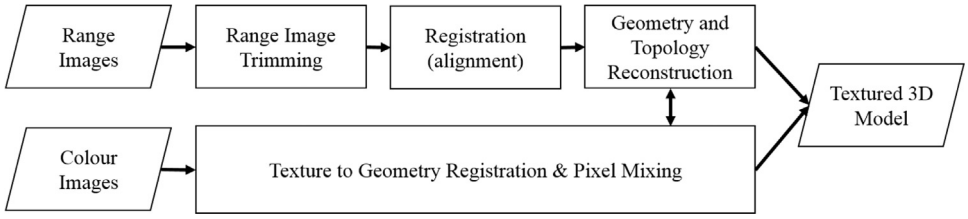

Fig. 2. Constructing a full 3D mesh model from several overlapping range scans including geometry and texture.

Table 1
Specifications for the NextEngine 3D Desktop Laser Scanner (NextEngine, 2015).

Hardware	
Unit dimensions	224×91×277 mm, 3.2 kg
Acquisition System	NextEngine proprietary MultiStripe Laser Triangulation
Laser	Twin arrays of four, Class 1 M, 10 mW solid state lasers, λ=650 nm
Sensor/Camera	Twin 5.0 Megapixel CMOS image sensors
Photo surface	Optically synchronous 7-colour surface capture
Photo lighting	Built-in whitelight
AutoDrive	Automatically controlled target platform, high precision, 9.1 kg max
Performance	
Target size	No limit, can align multiple scans together
Target field size	Macro mode, 130×97 mm; wide mode, 343×257 mm
Capture density	Up to 41 K points/cm^2 (macro mode), 4.5 K points/cm^2 (wide mode)
Texture density	500 DPI (macro mode), 200 DPI (wide mode)
Point accuracy	± 0.127 mm (macro mode), ± 0.381 (wide mode)

this study include rocks, minerals, and fossils and were scanned using the NextEngine™ 3D Desktop Laser Scanner (NextEngine, 2015). Specifications for the scanner can be seen in Table 1. Laser triangulation was used to capture a point cloud in a 'range image'. These images were 'trimmed' to remove any undesired portions. Sets of range images were collected and auto-aligned synchronously with photographic colour (i.e. texture) images. Individual range images and sets were then registered, or aligned, to a common 3D coordinate system (e.g. algorithms by Besl and McKay (1992), Chen and Medioni (1991), Zhang (1994)). Scanner software compensated for line-of-sight error (Bernardini and Rushmeier, 2002; Polo and Felicísimo, 2012). A final model of the scan was created in which the target's geometry and topology was reconstructed into a unified non-redundant surface. Throughout the process, texture (i.e. colour) values were registered to the geometry of the scan model through simultaneously captured colour images, where each point of the model point cloud was assigned a colour value (e.g. RGB). The colour values were mixed to get a representative depiction of the object. For more detail on the 3D model acquisition methodology see Bernardini and Rushmeier (2002). Colour can be a useful property in determining mineralogical composition of a sample. Its use as a diagnostic feature should be supported by other rock properties (e.g. crystal form, density, roughness, Moh's hardness, etc.), though the simple acquisition through texture mapping can be helpful in a first pass assessment of composition if no other properties are available.

Over 100 samples of rocks, minerals, and fossils were scanned to populate a database of virtual geological samples. A scan for a full model through the entire 3D model acquisition methodology can take between 20 and 40 min, depending on sample complexity and chosen point density. 3D model file size is typically on the scale of tens of megabytes, however there are numerous techniques available for file compression and cloud storage to mitigate this. Examples of 3D models of scanned samples can be seen in Fig. 3. The image on the left is an untextured core sample from a limestone quarry. Untextured here refers to the point cloud of the 3D sample without colour information, i.e. no coregistered RGB values. Cores are used in geotechnical disciplines for rock mass characterization by testing unconfined compressive strength (UCS). Documenting these samples digitally in this manner allows for sample-destructive laboratory procedures and the ability to compare different samples before and after testing (e.g. Head and Vanorio, 2016). The image on the right is of a granite sample from Skye, Scotland (from the Queen's University Rock and Mineral Museum Petrographic Collection). The sample is granite, which is defined as being composed of predominantly potassium feldspar, plagioclase feldspar, quartz, and also including biotite and/or amphibole. Granite is comparatively impervious and rigid, and has many geotechnical properties that make it favourable from a strength and stability perspective.

Each virtual sample in the prototype geological database is linked explicitly with its associated attributes, characteristic properties, and the geographic location of its origin. The spatial relationship among characteristics of scanned samples can be viewed in a macro-scale (e.g., GIS) environment as georeferenced features on a digital map.

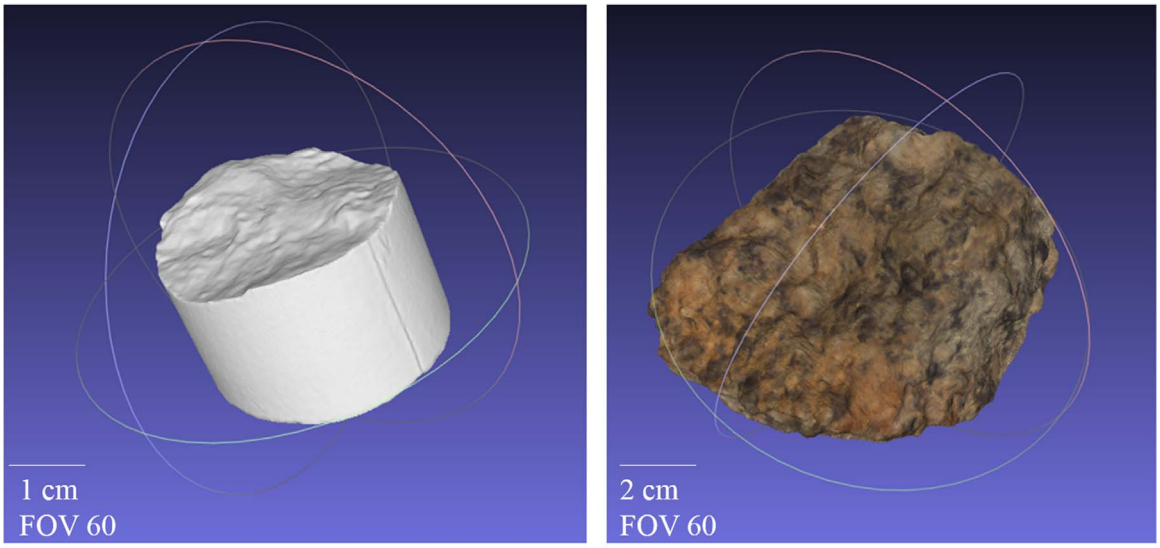

Fig. 3. Examples of 3D models of digitized geological samples from the developed virtual geological database, (a) shows an untextured piece of geotechnical core from a quarry in Bowmanville, Ontario, Canada, and (b) shows a granite sample collected in Skye, Scotland.

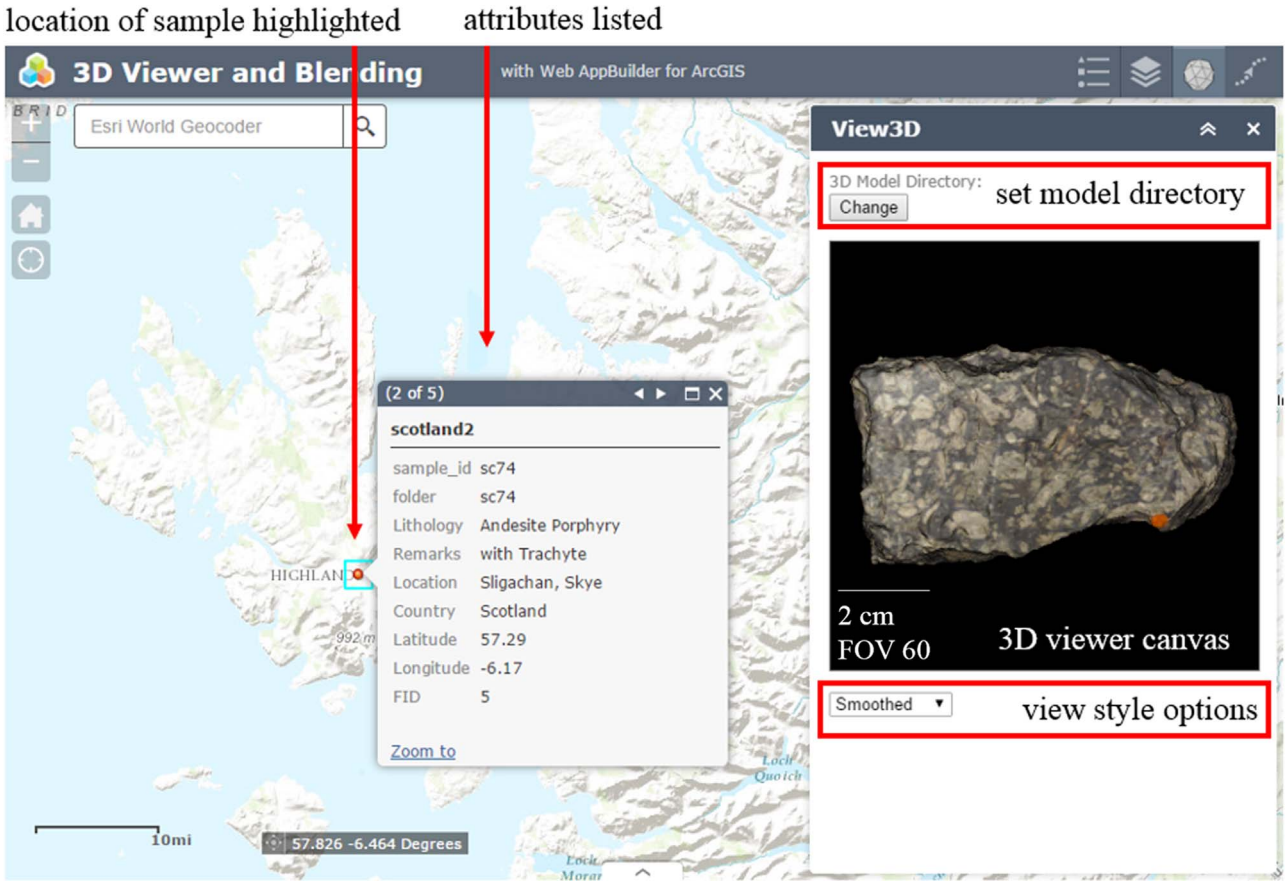

Fig. 4. 3D viewer widget along with the map interface for a case study in the Scottish highlands near where the Cuillin and Red Hills meet. This particular sample is an andesite porphyry. The location of the samples can be seen as points on the map. Style options can display the model in the following ways: point cloud, wireframe, flat, smoothed, or textured.

2.2. Custom widget development

In order to render the relationship between samples and their geographic locations on the Earth, two custom widgets were developed. The first widget focuses on the meso-scale, which is defined as hand-sized to outcrop size, and the second widget focuses on the macro-scale, which is defined as outcrop to larger size. The widgets are written in JavaScript and use the ArcGIS JavaScript API to communicate with the GIS components of the Web App.

The first widget's interface in the Custom Web App environment with its location highlighted as a selected point on the map can be seen in Fig. 4 and is based on the notion that the link between multi-scale observations should be facilitated through visual representation. This widget's main purpose is to show each 3D model linked with its

Table 2
Data sources for the macro-scale geophysical and geodetic images (USGS, 2000; OGS, 2011a, 2011b).

Feature	Source and Source Filename	Original Datum	Original Resolution
Digital Elevation Model (m)	USGS; SRTM n46_w081_1arc_v3	WGS84	30 m×30 m
Total Magnetic Intensity (nT)	OGS; ONMAGONL from GDS1036	NAD27	200 m×200 m
Bouguer Gravity (mGal)	OGS; ONGRAVITY from GD1036	NAD27	1000 m×1000 m

specified location on the Web App interface. In addition to showing a textured 3D model in the widget window, the user has the option to view the model as a non-textured point cloud and non-textured mesh as some geometric features can be less discernible when textured. The geologic hand sample shown in Fig. 4 is an andesite porphyry found close to where the Cuillin and Red Hills meet with basic extrusive rocks (Stephenson and Merritt, 2006). This geology is the result of a volcanic centre that was active during the Tertiary (ca. 70 Ma) at the proto-Atlantic rift (Evans et al., 2009). Andesites typically have a composition between rhyolite and basalt, and the porphyrytic texture evident in the sample is likely indicative of two-stages of cooling.

In addition to contextualized viewing and visual interpretation of meso-scale hand samples, visualization techniques may be applied to smaller scale datasets that arise from regional or global surveys of geophysical and geodetic data. Examples include magnetic, gravitational, radiometric, and spectral remotely sensed geophysical data. Here, magnetic (total magnetic intensity in nanoteslas, nT), gravity (Bouguer anomaly in milliGals, mGal), and topography (elevation in metres above sea level, m) datasets of the Sudbury region in Ontario, Canada, were viewed in the interactive interface. All datasets use grayscale legends, with darker pixels corresponding to lower values and lighter pixels corresponding to higher values for each data type's respective units. Kovesi et al. (2014) have explored the concept of multi-image blending of similar geophysical datasets through the weighting of each image's influence on a final image. In contrast, this study approaches the concept differently by varying, if defined, the opacity of the data which allows for simultaneous visualization of the underlying basemap in the Web App. Blending presents an opportunity to view multiple datasets simultaneously and to assess how they correspond in an interactive and visual manner in an ArcGIS Web App (which is a new utility for this platform). The geophysical and geodetic data used in this paper are summarized in Table 2 and the widget interface is introduced in Fig. 5 with elevation shown at full visibility. The blending widget interface is also shown. An example that demonstrates how the blending works follows.

The application of this visualization technique is useful in viewing how layers relate to one another and to the underlying landscape. This relationship serves to improve the understanding of spatial relationships among geophysical and geodetic data. Practical applications can reveal relationships among datasets visually and intuitively for a user, which may lead to interpreting possible geological relationships in the region given the geometry of these trends. For datasets used for ore body exploration, such as total magnetic intensity and Bouguer anomaly, potential ore bodies may be revealed by synthesizing the corresponding value intensities and geometric relationships, as illustrated in Case Study 2.

The blending widget can be modified based on the number and which layers are to be blended. The widget's interface includes a section called the blending area. This can be seen in Fig. 6. The opacity of selected layers is modifiable based on the cursor's position within the blending area relative to the origin in the top left corner of the square. The three blending area configurations are shown in Fig. 7 along with corresponding equations that show how the opacity value is calculated.

The equations below show how opacity values are calculated for the blending areas seen in Fig. 7 as follows:

$$\alpha_X = \frac{h_{cursor}}{h_{tot}} \tag{1}$$

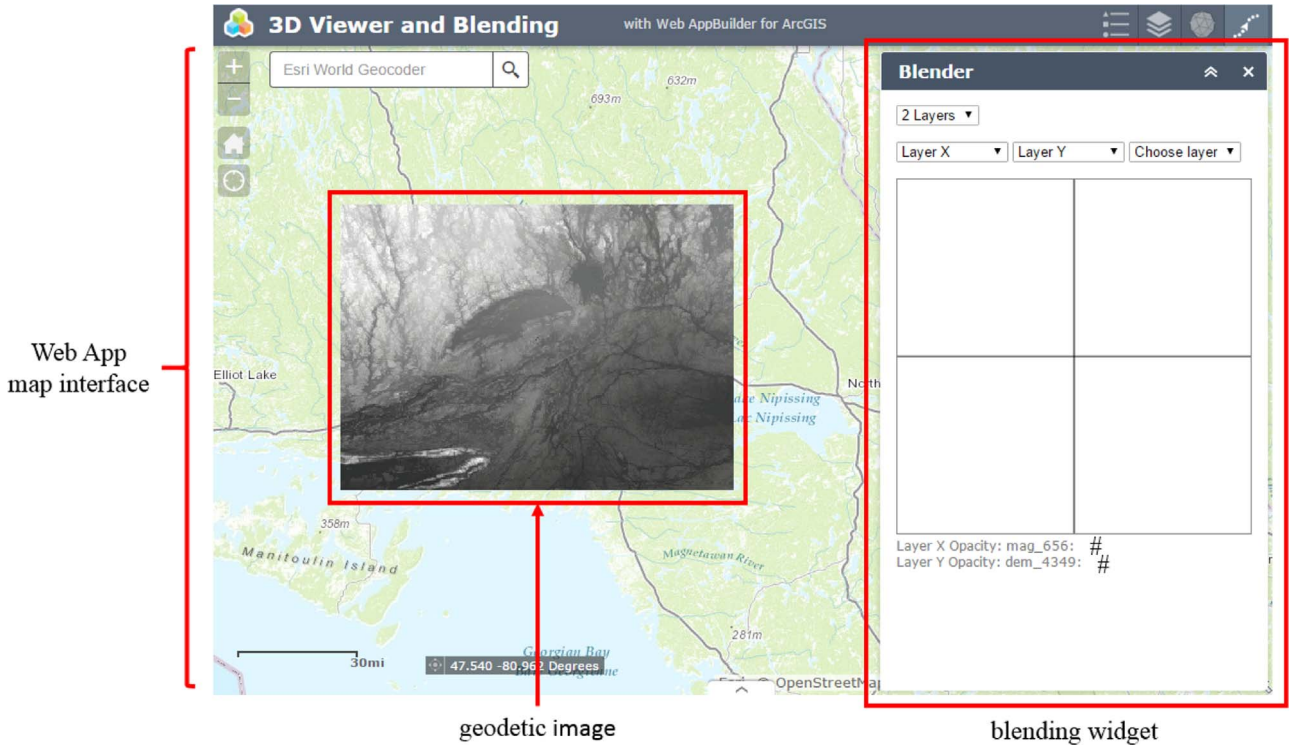

Fig. 5. Geophysical and geodetic maps of Sudbury, Ontario, Canada. Tile Layers brought into a Custom Web App where the blending widget can be used to change the opacity values and "blend" the images. Digital elevation is shown with darker cells referring to lower elevation.

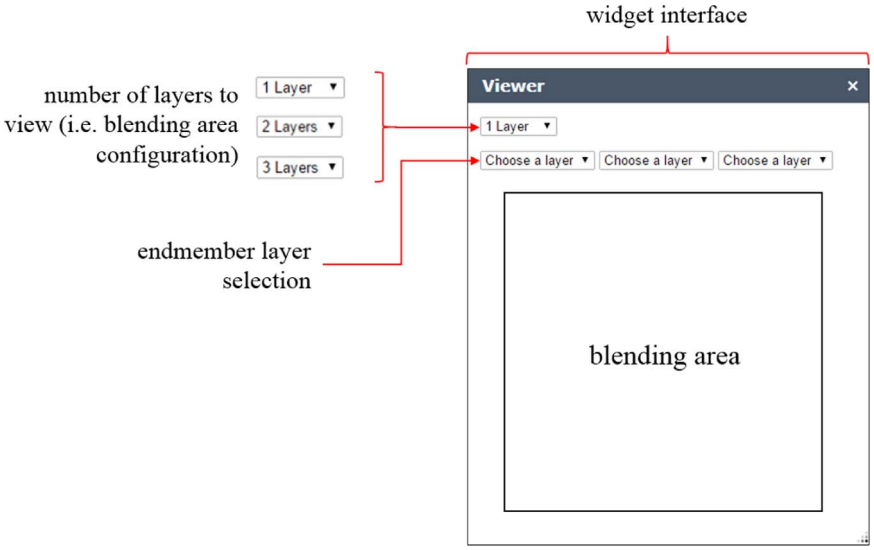

Fig. 6. The widget interface for blending geophysical and geodetic images. The user has the option to select the number of layers to be blended and to select which layers to blend and view. The blending area interface corresponds to Fig. 7(a)–(c) with respect to the number of layers selected.

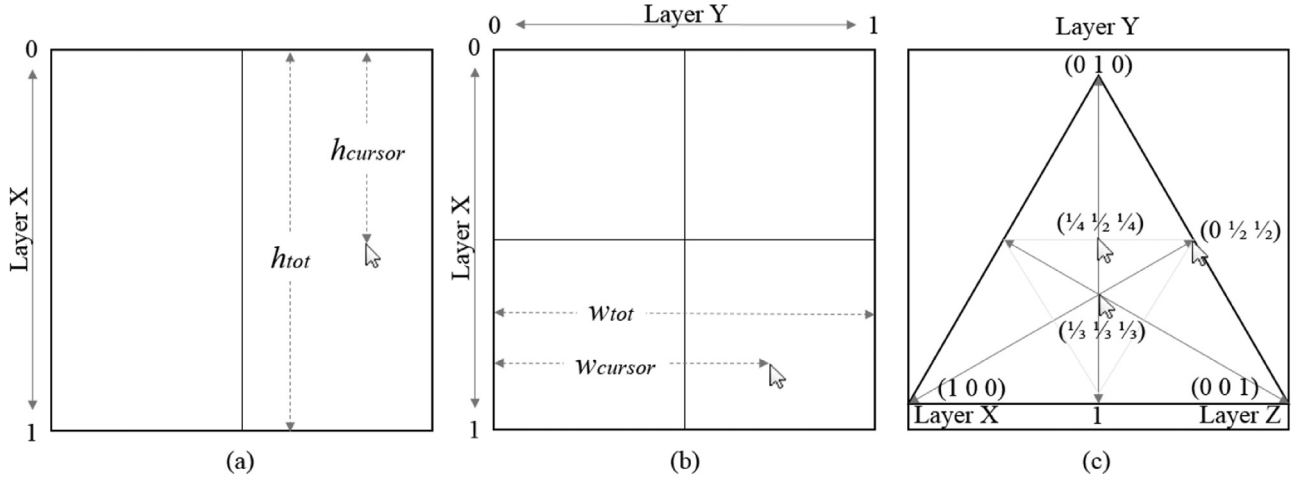

Fig. 7. Interfaces for the blending area, (a) is for one layer, where the vertical axis represents the opacity of the chosen layer, (b) is for two layers, where each axis represents the opacity of the layers, and (c) is for three layers where opacity is calculated based on the cursor's barycentric coordinates. There are some keys coordinates labelled.

$$\alpha_Y = \frac{w_{cursor}}{w_{tot}} \tag{2}$$

where, α_x is opacity of layer X in configurations (a) and (b), α_y is the opacity of layer Y in configuration (b), h_{cursor} is the cursor's vertical distance relative to the origin and total height, h_{tot}, of the blending area, and w_{cursor} is the cursor's horizontal distance relative to the origin and total width, w_{tot}, of the blending area. The opacity of layers X, Y, and Z in configuration (c) are based on the same relationship of the cursor's position relative to each endmember position. Configuration (c) shows some examples of key barycentric coordinates with opacity values given.

The following example in Fig. 8(a)–(f) shows how the blending widget interface works for a two layer blend, with each subfigure including the cursor's position in the blending area and the corresponding images with adjusted opacity. The example is again of the Sudbury region and looks at the magnetic and topographic datasets. The example follows the progression of full opacity of both images (a), transitioning to full visibility of the magnetic layer (b)–(c), to a mix between the magnetic and topographic layers (d)–(e), to full visibility of the topographic layer (f).

Combining the ArcGIS Online platforms with 2D and 3D visualization tools results in an interactive and intuitive interface for interacting with digitized meso-scale geological samples and macro-scale geophysical and geodetic data. Viewing datasets using the described widgets allows for a variety of applications. Two case studies that show further practical applications in geology are presented below.

3. Case study 1: 3D sample viewer

Kingston, Ontario, Canada, and the surrounding regional geology is dominantly composed of Precambrian age basement rocks along a northwest-southeast trending ridge known as the Frontenac Axis with Paleozoic sedimentary rocks flanking on either side. During the Grenville orogeny 1100 million years ago, limestone, sandstone, and mud-sandstones were metamorphosed into marble, quartzite, and gneissic rocks, respectively, of the granulite facies. Contemporaneous volcanism resulted in plutonic bodies of basic, granitic, and syenitic rocks, and diabase and porphyritic andesitic dykes (Hewitt, 1964). The mountains from this orogenic event were eroded over the following 500 million years (Greggs and Gorman, 1976; Wynne-Edwards, 1967), followed by unconformably laying Cambro-Ordovician siltstones, sandstones, limestones, and dolostones (Kirwan, 1963; Armstrong and Dodge, 2007).

A sample found within the Kingston region was scanned and placed within geological and geographic context. The sample, along with

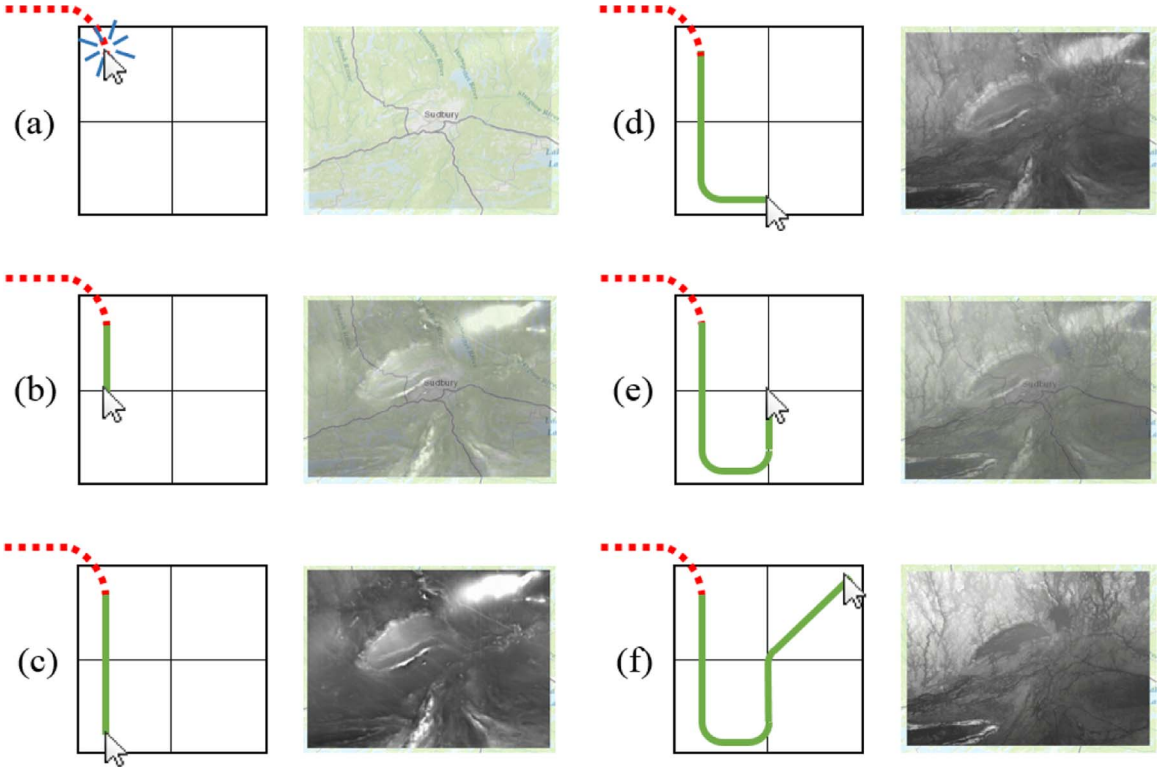

Fig. 8. A depiction of blending of total magnetic intensity data (TMI, nT), and a digital elevation model (DEM, m). (a) Shows almost full opacity of both layers. The blending is activated when the cursor clicks on the blending area. (b)–(c) shows the magnetic layer transitioning towards full visibility. (d) Shows complete mixing of the two layers. (e) Shows equal mixing of both layers, however they both have 0.5 opacity and the basemap can be seen. (f) Shows topography as fully visible and the magnetic layer at full opacity.

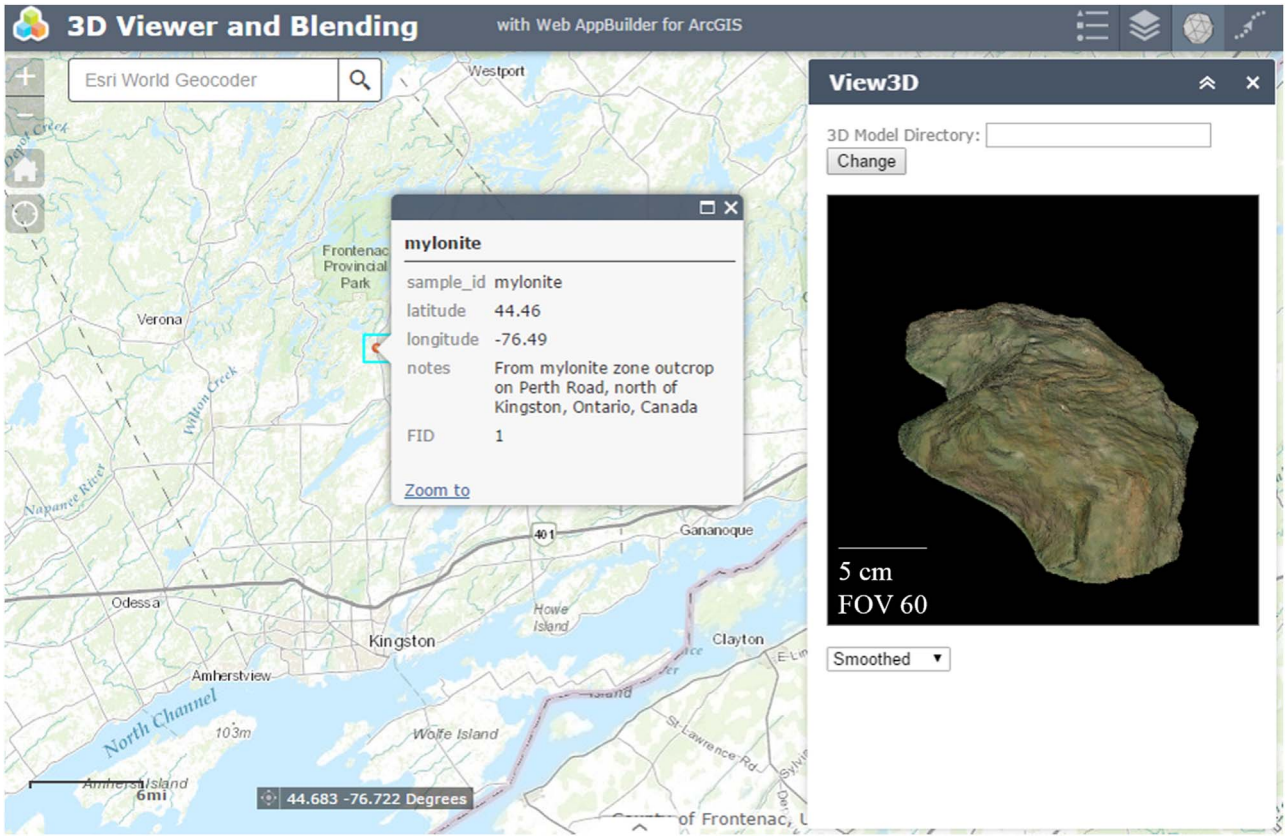

Fig. 9. The 3D viewing widget and Web App. The sample appears after its point is clicked within the map. The sample can be rotated, zoomed in and out from for further inspection. (For interpretation of the references to color in this figure legend, the reader is referred to the web version of this article.)

Fig. 10. Paragneiss sample from the Perth Road mylonitic outcrop. Note the intense anastomosing fold bands within the sample, highlighted in the first view in red. Scale information is shown for the first depiction.

Table 3
Three important ore minerals in the Sudbury Structure region (including formulas, specific gravities (unitless), and relative magnetic susceptibilities).

Mineral	Formula	Specific Gravity	Magnetism
pyrrhotite	$Fe_{1-x}S$ (x=0–0.2)	4.58–4.65	strong
pentlandite	$(Fe,Ni)_9S_8$	4.6–5	non-magnetic
chalcopyrite	$CuFeS_2$	4.1–4.3	magnetic after heating

associated attributes, is exemplary of a number of features associated with the local geology and how it fits into the geological evolution of North America based on metamorphic petrological history and structural history. Fig. 9 shows the sample and its location with respect to the city of Kingston. The sample is found in the mylonite zone outcrop on Perth Road north of Kingston (specifically at 44°27′52″N and 76°29′29″W - see popup). The sample shows gneissic banding highlighted in red. The sample contain minerals that are indicative of a low grade metamorphism formational environment. Mylonitization occurred after the severe regional metamorphism and regional gneissosity had peaked. The intense mylonitization occurs in the paragneiss unit and has an irregular distribution and width of anastomosing bands. The foliation strikes northeast and has a steeply-plunging extension lineation found on the mylonitic foliation planes (Ermanovics, 1967). The sample in the 3D viewer in several orientations can be seen in Fig. 10. The gneissic banding is highlighted with the red line in the first view. For further details on the geology, see Harvey (2016).

The described geology of the area includes a few of the properties that are inherently part of the sample and deduced from visual interpretation of it in the online viewer. It is exemplary of the mylonitic rock structures in the area, providing insight to the geological paleoenvironment formational model that describes it in a certain point in time. Virtually accessing and visualizing this outcrop by proxy as well as other locations worldwide could allow for analogues and comparisons to other geological areas.

4. Case study 2: multi-modal geophysical and geodetic image blending

This case study looks at the Sudbury Structure in Ontario, Canada. It is composed of three main components which are (1) the Sudbury Basin consisting of Precambrian sediments and volcanics, (2) the Sudbury Igneous Complex (SIC), which is a lopolitic structure surrounding the basin, and (3) a surrounding zone of brecciated footwall rocks. This region has historically been and continues to be of great economic interest for the Canadian mining and resources industry as some of the world's largest Ni-Cu-PGE magmatic sulphide deposits occur in host rocks at or near the base of the SIC (Rousell and Card, 2009). The structure is widely believed to have formed as a result of a meteorite impact during the Paleoproterozoic era and subsequent orogenic events causing deformation to the north-east trending ellipse shape at surface. Major ore minerals in the SIC and associated physical properties are listed in Table 3.

The case study shows how the blending widget of the online Web App can be used to find similarities among different types of datasets. Here, total magnetic intensity (TMI, nT), elevation (m), and Bouguer gravity (mGal) datasets are uploaded into the Web App. Each endmember is located at a vertex of the blending ternary diagram, and the visibility weighting is shown underneath the blending area. For each dataset image, darker cells indicate lower intensity values and lighter cells indicate higher intensity values, all with respect to each dataset's units and each dataset's maximum and minimum values. Fig. 11 shows each of the endmembers labelled, where each is at full visibility (i.e. opacity =0). The red circle depicts the ellipse shape of the Sudbury Structure at surface.

The crater shape can be seen in the elevation endmember, where a dark oval shape is visible. This is where impact would have occurred. This oval shape can also be seen in both the magnetic and gravity endmembers. Additionally, a strong magnetic anomaly is visible along the southern rim, which coexists in plan view with a higher gravity anomaly signal. Magnetic and gravity anomalies coexisting can be

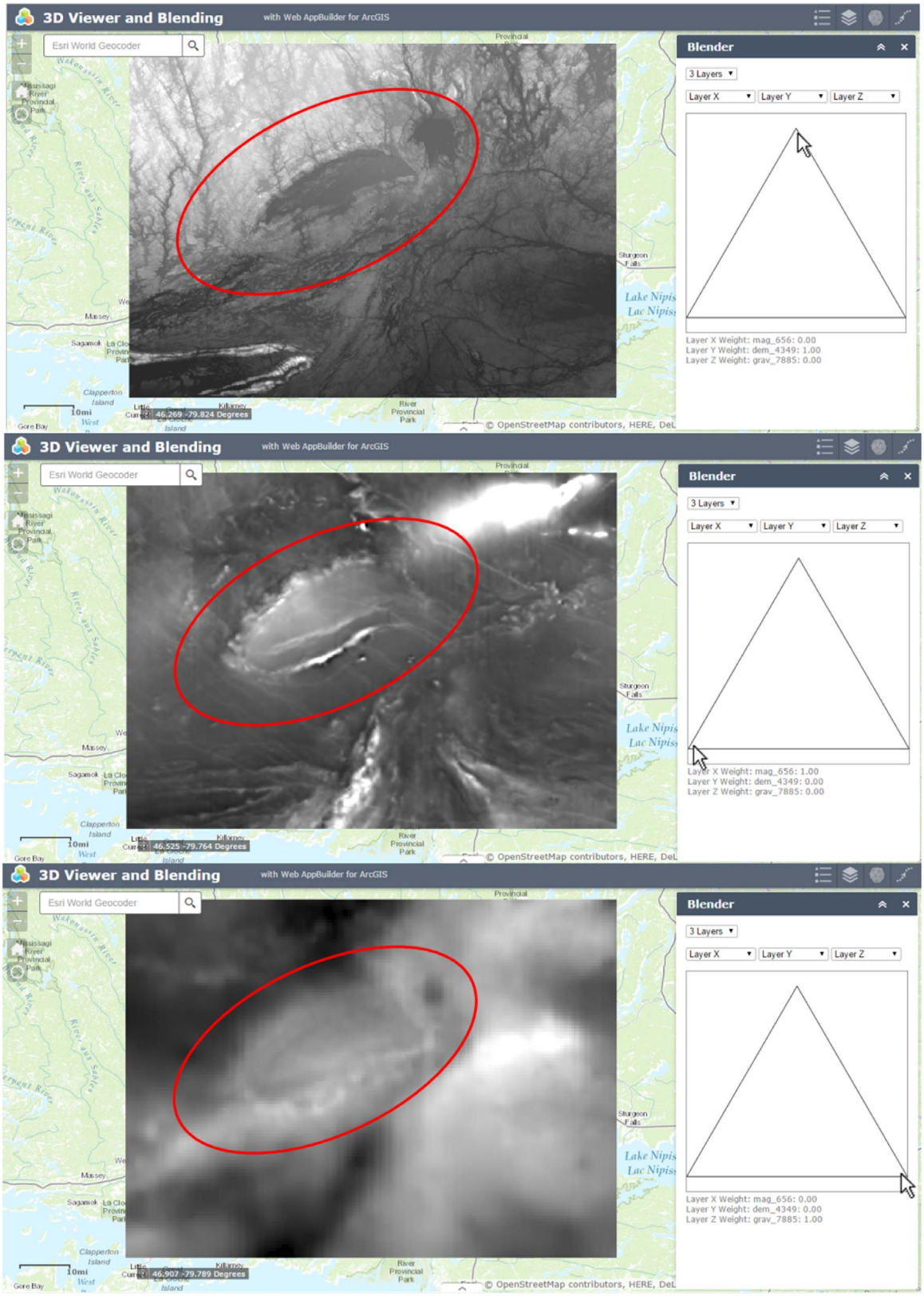

Fig. 11. Three geophysical/geodetic datasets used in Case Study 2. Top: elevation (m), Middle: total magnetic intensity (nT), Bottom: Bouguer gravity (mGal). Red ellipse: the Sudbury Structure seen at surface, which is visible for each dataset. (For interpretation of the references to color in this figure legend, the reader is referred to the web version of this article.)

indicative of mineralizations of economic resources. The specific gravity of crustal rocks is averaged to be approximately 2.75, which is lower in comparison to the aforementioned major ore minerals. The presence of high density minerals would result in a high gravity reading compared to surrounding host rocks. Pyrrhotite is strongly magnetic relative to generally non-magnetic typical crustal rocks. Fig. 12 shows the gravity and magnetic datasets viewed simultaneously. Along the southern rim of the SIC, higher magnetic and gravity values can be

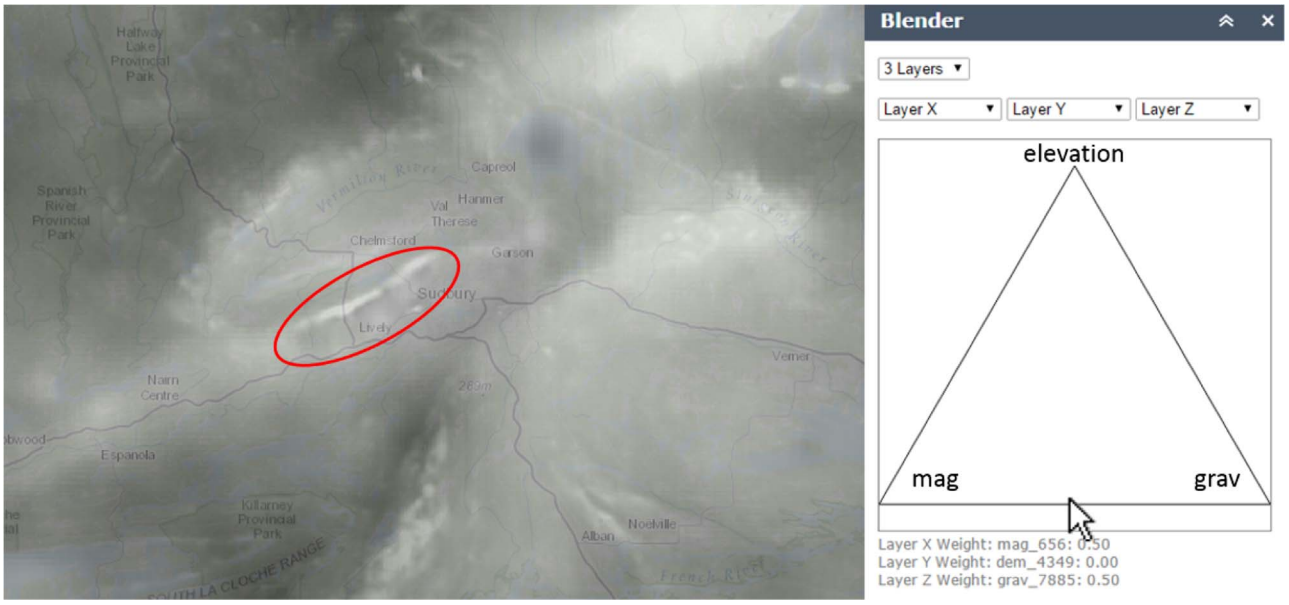

Fig. 12. Magnetic and gravity datasets both at opacity=0.5. Elevation is not visible in this figure based on the cursor's position in the blending widget. Red ellipse shows an area where total magnetic intensity and Bouguer gravity have higher values and overlay. (For interpretation of the references to color in this figure legend, the reader is referred to the web version of this article.)

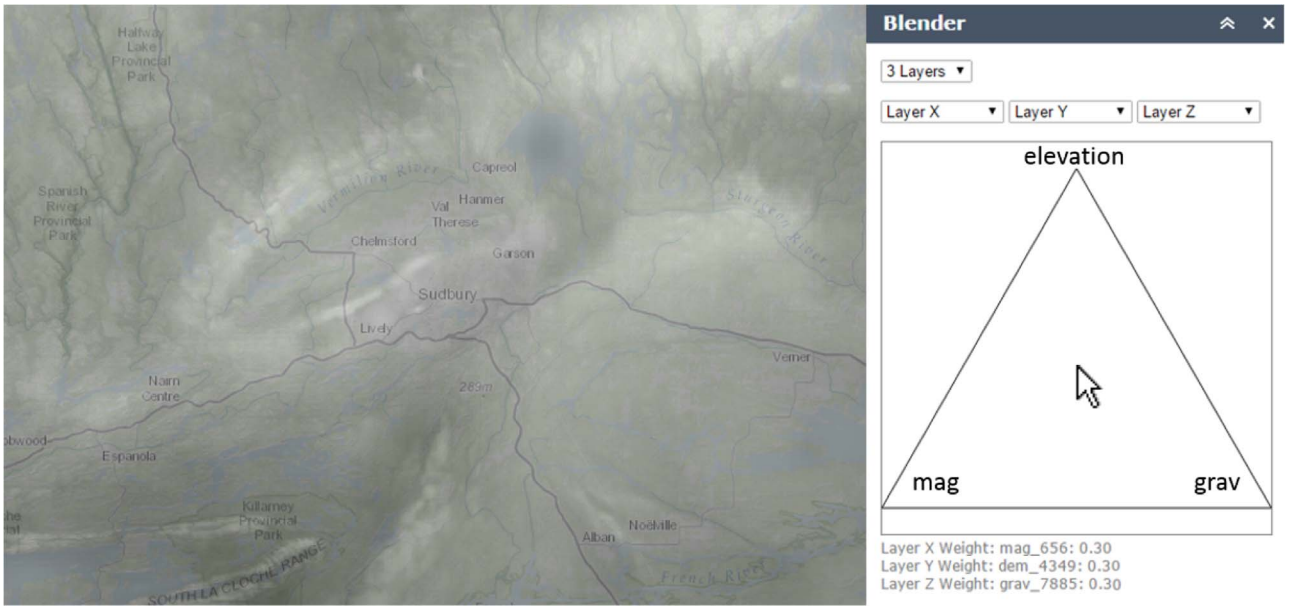

Fig. 13. Three geophysical/geodetic datasets viewed simultaneously; each with a visibility of 0.3. This allows for contextualization of the data within the underlying basemap.

seeing, implying that minerals that have strong signatures for this type of geophysical response coexist here. This offers an opportunity to easily view and visually interpret the datasets together, whereas a traditional approach may require more steps to view each aspect separately, and possibility even non-digitally.

The interactive blender helps a user to view rapidly all three end-members and simultaneously view more than one layer dynamically. In this case study, layer opacity is modified to change how the layer is viewed. This is in contrast to Kovesi et al. (2014), who used proportions to change the weighting of an image. In the present case, opacities are used such that interaction and visibility of the underlying basemap is possible for further contextualization. The ellipse shape is visible in all three, which is beneficial to characterize the region geophysically, understand the geological history, and explore possible economic resources. Fig. 13 shows all three layers at the same opacity (visibility=0.3). Static images do not fully convey the effectiveness of the tool, as it has been designed to be dynamic and interactive, though similar overlying trends can be seen among the images.

In contrast to the coexisting magnetic and gravity signals in the southern portion of the SIC, the Temagami magnetic anomaly is distinct with regards to other portions of the magnetic map. While gravity signals are higher in this region, it is clear that there are other regions on the map with higher gravity values, not evident for the Temagami anomaly, which covers a large area and has a high magnetic signal. The Temagami area, however, has not seen the mining activity that the Sudbury Structure has. Fig. 14 compares the magnetic and gravity images.

The widget allows for maintaining the user's focus on data trends and images and offers the ability to quickly compare heterogeneous datasets that may correlate, adding to the geologist's toolbox of approaches for interpretation of samples and their surrounding geology.

Fig. 14. Images of the Sudbury Structure offset to the left of centre for each, and the Temagami anomaly in the top right corners. The left image is of the magnetic data and the right image is of the gravity data. The red ellipse highlights the mentioned magnetic anomaly, which is clearly is the largest highly magnetic portion of the map. The yellow ellipse shows an area with low magnetic values but a higher gravity anomaly. (For interpretation of the references to color in this figure legend, the reader is referred to the web version of this article.)

5. Discussion of results

It is acknowledged that direct interaction with geological samples offers advantages over digital methods in assessing various diagnostic features required for full comprehension in geology. The range at which humans can directly observe geological phenomena is narrow and the unification and abstraction of multi-scale data and different types of data into a common platform presents an opportunity to ease cognitive load in the user comprehension of associated complexities. These visualization tools can aid in augmenting user comprehension of spatial relationships and offer flexibility in database exploration, visualization, management, and archiving in a well-known GIS environment.

The physical storage space required for physical samples, as indicated by the USGS Geological Collections Management System, is substantial and the tools presented above can supplement physical archiving requirements and reduce strain on the system as a whole. Additionally, once samples are digitally archived and available as 3D models worldwide, researchers, educators, and field geologists can have immediate access to an enormous database. Paleogeographic environments are often presented as general models of formation (noting that all models are representations with bias and uncertainty). Formational analogues for geological settings may exist elsewhere in the world. In the future, with a highly populated database, accessing these samples rapidly and digitally can facilitate important decisions (i.e., phase one site investigation).

The infrastructure to hold the 3D files would be considerably smaller than that of physical samples. However, large 3D file sizes may not be suitable for immediate download upon opening of the Web App. A select-and-download interface from a database may suit the Web App well, as accessing cloud storage could take up time when loading each sample in contrast to loading each sample from a user's machine. Regardless of how long the 3D file takes to load, they are immediately responsive in the 3D viewer window, allowing for quick visual interpretation.

Every case of geological investigation is different requiring various sets of data in the assessment process. The two widgets developed and described in this paper are examples of useful applications that can see applicability in a variety of geological investigations. The common platform-modular approach to multi-scale visualization in geoscience offers a high degree of flexibility and universality in the research and education communities. This allows for a balance between visual conceptualization (e.g. of 3D photorealistic hand samples) and abstracted 2D analytical techniques.

6. Conclusions

This paper demonstrates the utility of intersecting 3D acquisition and geovisualization for geological data at multiple scales. A database of virtual geological samples was populated using a data acquisition procedure for meso-scale geological hand samples of rocks, minerals, and fossils. These samples were brought into an online GIS environment to view their georeferenced locations and to provide geospatial context for users. This was done by building a widget for an ArcGIS Web App allowing 3D samples to be selected via their basemap macro-scale features for viewing. A case study showed these as foundational components for a globally accessible database of virtual geological samples. A second widget was built to simultaneously view heterogeneous geophysical datasets through blending. This approach was not previously available for this platform and was implemented to provide further geological context for the multi-scale synthesis of datasets permissible in this interface. While tools presented in this paper emphasize visualization, the opportunity to utilize the widgets and 3D samples for quantitative analysis is possible and is the focus of future work.

Acknowledgments

This research was funded through an NSERC Engage Grant to the second author. Mark Badham of the Miller Museum of Geology, Queen's University and Mark Diederichs are thanked for the geological samples provided for the case study. Rebecca Hudson is thanked for 3D scanning of geological samples. The anonymous reviewers are also thanked for their valuable input that improved the final version of this manuscript.

References

Armstrong, D.K., Dodge, J.E.P., 2007. Paleozoic Geology of Southern Ontario – Project Summary and Technical Document. Ontario Geological Survey, Miscellaneous Release–Data 219.

Baker, B.R., Gessner, K., Holden, E.J., Squelch, A.P., 2008. Automatic detection of anisotropic features on rock surfaces. Geosphere 4 (2), 418. http://dx.doi.org/10.1130/GES00145.1.

Bates, K., Falkingham, P., Rarity, F., 2010. Application of high-resolution laser scanning and photogrammetric techniques to data acquisition, analysis and interpretation in palaeontology. Int. Arch. Photogramm. Remote Sens. Spat. Inf. Sci. XXXVIII (5), 68–73.

Bernardini, F., Rushmeier, H., 2002. The 3D model acquisition pipeline. Comput. Graph. Forum 21 (2), 149–172. http://dx.doi.org/10.1111/1467-8659.00574.

Besl, P., McKay, N., 1992. A method for registration of 3-D shapes. IEEE Trans. Pattern Anal. Mach. Intell. 14 (2), 239–256. http://dx.doi.org/10.1109/34.121791.

Betts, M.W., Maschner, H.D.G., Schou, C.D., Schlader, R., Holmes, J., Clement, N., Smuin, M., 2011. Virtual zooarchaeology: building a web-based reference collection of northern vertebrates for archaeofaunal research and education. J. Archaeol. Sci. 38 (4), 755–762. http://dx.doi.org/10.1016/j.jas.2010.06.021.

Blenkinsop, T.G., 2012. Visualizing structural geology: from excel to Google Earth. Comput. Geosci. 45, 52–56. http://dx.doi.org/10.1016/j.cageo.2012.03.007.

British Geological Survey, 2016. GB3D Type Fossils Online Project. ⟨http://www.3d-fossils.ac.uk/⟩.

Byers, C., Woo, A., 2015. 3D data visualization: the advantages of volume graphics and big data to support geologic interpretation. Interpretation 3 (3), 29–39. http://dx.doi.org/10.1190/INT-2014-0257.1.

Cai, W., Sakas, G., 1999. Data intermixing and multi-volume rendering. Comput. Graph. Forum 18, 359–368.

Chávez, G.M., Sarocchi, D., Santana, E.A., Borselli, L., Rodríguez-Sedano, L.A., 2014. Using Kinect to analyze pebble to block-sized clasts in sedimentology. Comput. Geosci. 72, 18–32. http://dx.doi.org/10.1016/j.cageo.2014.07.008.
Chen, Y., Medioni, G., 1991. Object modelling by registration of multiple range images. Proceedings of the 1991 IEEE International Conference on Robotics and Automation, CH2969(4), 2724–2729.
Çöltekin, A., Lokka, I., Zahner, M., 2016. On the usability and Usefulness of 3D (Geo) visualizations – a focus on virtual reality environments. Int. Arch. Photogramm. Remote Sens. Spat. Inf. Sci. Commun.. http://dx.doi.org/10.5194/isprs-archives-XLI-B2-387-2016.
Contessi, M., Fanti, F., 2012. Vertebrate tracksites in the middle Jurassic-upper Cretaceous of South Tunisia. Ichnos 19, 211–227. http://dx.doi.org/10.1080/10420940.2012.711396.
De Paor, D.G., 2016. Virtual rocks. GSA Today 8, 4–11. http://dx.doi.org/10.1130/GSATG257A.1.
Domingo, I., Villaverde, V., López-Montalvo, E., Lerma, J.L., Cabrelles, M., 2013. Latest developments in rock art recording: towards an integral documentation of Levantine rock art sites combining 2D and 3D recording techniques. J. Archaeol. Sci. 40 (4), 1879–1889. http://dx.doi.org/10.1016/j.jas.2012.11.024.
Ermanovics, I.F., 1967. Evidence Bearing on the Origin of the Perth Road Pluton, Southern Ontario (Ph.D. thesis). Queen's University, Kingston, Ontario, Canada.
Evans, J., Montgomery, J., Wildman, G., 2009. Isotope domain mapping of 87Sr/86Sr biosphere variation on the Isle of Skye, Scotland. J. Geol. Soc. 166 (1985), 617–631. http://dx.doi.org/10.1144/0016-76492008-043.
Fanti, F., Contessi, M., Nigarov, A., Esenov, P., 2013. New data on two large dinosaur tracksites from the upper Jurassic of Eastern Turkmenistan (Central Asia). Ichnos 20, 54–71. http://dx.doi.org/10.1080/10420940.2013.778845.
Geologic Materials Repository Working Group, 2015. The U.S. Geological Survey Geologic Collections Management System (GCMS): A Master Catalog and Collections Management Plan for U.S. Geological Survey Geologic Samples and Sample Collections: Circular 1410. Reston, VA. doi: http://dx.doi.org/10.3133/cir1410.
Greggs, R.G., Gorman, W.A., 1976. Geology of the 1000 Islands. Parks Canada. Retrieved from ⟨http://www.oliverkilian.com/ecology/thousand-islands/island-insights/geology/rocks.html#Landforms⟩.
Harvey, A.S., 2016. Multi-Scale Visualization and Interpretation of Geological Relationships, MASc Thesis. Queen's University, Kingston, Ontario, Canada.
Head, D., Vanorio, T., 2016. Effects of changes in rock microstructures on permeability: 3-d printing investigation. Geophys. Res. Lett. 43, 1–9. http://dx.doi.org/10.1002/2016GL069334.Received.
Hewitt, D.F., 1964. Geological Notes for Maps Nos. 2053 and 2054 Madoc-Gananoque Area. Ontario Geological Survey, Geological, 1–42.
Jordan, C.J., Napier, B., 2016. Developing digital fieldwork technologies at the British Geological Survey. Geological Society, London, Special Publications 436, 1–11. http://dx.doi.org/10.1144/SP436.6.
Khoshelham, K., Elberink, S.O., 2012. Accuracy and resolution of kinect depth data for indoor mapping applications. Sensors 12, 1437–1454. http://dx.doi.org/10.3390/s120201437.
King, C., 2008. Geoscience education: an overview. Stud. Sci. Educ. 44 (2), 187–222. http://dx.doi.org/10.1080/03057260802264289.
Kirwan, J.L., 1963. The age of the Nepean (Potsdam) sandstone in eastern Ontario. Am. J. Sci. 261, 108–110.
Kovesi, P., Holden, E., Wong, J., 2014. Interactive multi-image blending for visualization and interpretation. Comput. Geosci. 72, 147–155. http://dx.doi.org/10.1016/j.cageo.2014.07.010.
Kuzminsky, S.C., Gardiner, M.S., 2012. Three-dimensional laser scanning: potential uses for museum conservation and scientific research. J. Archaeol. Sci. 39 (8), 2744–2751 . http://dx.doi.org/10.1016/j.jas.2012.04.020.
Lin, S.C.H., Douglass, M.J., Holdaway, S.J., Floyd, B., 2010. The application of 3D laser scanning technology to the assessment of ordinal and mechanical cortex quantification in lithic analysis. J. Archaeol. Sci. 37 (4), 694–702. http://dx.doi.org/10.1016/j.jas.2009.10.030.
MacEachren, A.M., Kraak, M., 1997. Exploratory cartographic visualisation: advancing the agenda. Comput. Geosci. 23 (4), 335–343. http://dx.doi.org/10.1002/9780470979587.ch11.
MacEachren, A.M., Gahegan, M., Pike, W., Brewer, I., Cai, G., Lengerich, E., Hardisty, F., 2004. Geovisualization for knowledge construction and decision support. IEEE Comput. Graph. Appl. 24 (1), 13–17.
Mankoff, K.D., Russo, T.A., 2013. The kinect: a low-cost, high-resolution, short-range 3D camera. Earth Surf. Process. Landf. 38, 926–936. http://dx.doi.org/10.1002/esp.3332.
Mills, G., Fotopoulos, G., 2013. On the estimation of geological surface roughness from terrestrial laser scanner point clouds. Geosphere 9 (5), 1410–1416. http://dx.doi.org/10.1130/GES00918.1.
Mookerjee, M., Vieira, D., Chan, M.A., Gil, Y., Pavlis, T.L., Spear, F.S., Tikoff, B., 2015. Field data management: integrating cyberscience and geoscience. EOS Earth Space Sci. News 96, 20.
NextEngine, 2015. Retrieved May 20, 2015, from ⟨http://www.nextengine.com/⟩.
Ontario Geological Survey, 2011a. 1:250 000 scale bedrock geology of Ontario. Ontario Geological Survey, Miscellaneous Release - Data 126 - Revision 1.
Ontario Geological Survey, 2011b. Single master gravity and aeromagnetic data for ontario. Ont. Geol. Surv. Minist. North. Dev. Mines, 1035.
Polo, M.E., Felicísimo, A.M., 2012. Analysis of uncertainty and repeatability of a low-cost 3D laser scanner. Sensors 12, 9046–9054. http://dx.doi.org/10.3390/s120709046.
Porter, T., Duff, T., 1984. Compositing digital images. SIGGRAPH 18 (3), 253–259.
Qiu, S., He, B., Bai, X., Li, X., Liao, Z., Yin, C., 2015. A mineral resources quantiative assessment and 3D visualization system. IEEE International Geoscience and Remote Sensing Symposium (IGARSS). 2015 IEEE.
Rousell, D.H., Card, K.D., 2009. Sudbury Area Geology and Mineral Deposits. A Field Guide to the Geology of Sudbury, Ontario. pp. 1–5.
Sanchez, C.A., 2012. Enhancing visuospatial performance through video game training to increase learning in visuospatial science domains. Psychon. Bull. Rev. 19, 58–65. http://dx.doi.org/10.3758/s13423-011-0177-7.
Sims, V.K., Mayer, R.E., 2002. Domain specificity of spatial expertise: the case of video game players. Appl. Cogn. Psychol. 16, 97–115. http://dx.doi.org/10.1002/acp.759.
Sivarajah, Y., Holden, E.J., Togneri, R., Price, G., Tan, T., 2014. Quantifying target spotting performances with complex geoscientific imagery using ERP P300 responses. Int. J. Hum. Comput. Stud. 72 (3), 275–283. http://dx.doi.org/10.1016/j.ijhcs.2013.10.007.
Stephenson, D. (BGS), Merritt, J. (BGS), 2006. Skye a Landscape Fashioned by Geology. Scottish Natural Heritage. British Geological Survey. Retrieved from ⟨http://saifollahi.persiangig.com/1559636882.pdf#page=214⟩.
United States Geological Survey, 2000. Shuttle Radar Topography Mission 1 Arc-Second Global Elevation Data.
Uttal, D.H., Cohen, C.A. 2012. Spatial Thinking and STEM Education. When, Why, and How? Psychology of Learning and Motivation Advances in Research and Theory. 57, 147-181. http://dx.doi.org/10.1016/B978-0-12-394293-7.00004-2.
Westoby, M.J., Brasington, J., Glasser, N.F., Hambrey, M.J., Reynolds, J.M., 2012. "Structure-from-Motion" photogrammetry: a low-cost, effective tool for geoscience applications. Geomorphology 179, 300–314. http://dx.doi.org/10.1016/j.geomorph.2012.08.021.
Whitmeyer, S.J., Nicoletti, J., De Paor, D.G., 2010. The digital revolution in geologic mapping. GSA Today 20 (4), 4–10. http://dx.doi.org/10.1130/GSATG70A.1.
Wu, H.K., Shah, P., 2004. Exploring visuospatial thinking in chemistry learning. Sci. Educ. 88, 465–492. http://dx.doi.org/10.1002/sce.10126.
Wynne-Edwards, H.R., 1967. Westport map-area, Ontario, with special emphasis on the Precambrian rocks. Geol. Surv. Can., Mem. 346, 144.
Yeniceli, S., Ozcelik, M., 2016. Practical application of 3D visualization using geotechnical database: a case study Karsiyaka (Izmir) settlement area (Turkey). J. Indian Soc. Remote Sens. 44, 129–134. http://dx.doi.org/10.1007/s12524-015-0474-0.
Zhang, Z., 1994. Iterative point matching for registration of free form curves and surfaces. Int. J. Comput. Vis. 12 (1994), 119–152.
Zlatanova, S., 2008. Working Group II – acquisition – position paper: data collection and 3D reconstruction. In: Advances in 3D Geoinformation Systems. Springer Berlin Heidelberg. pp. 425–428.